Defects in GPI biosynthesis perturb Cripto signaling during forebrain development in two new mouse models of holoprosencephaly

David M. McKean and Lee Niswander*

HHMI, Department of Pediatrics, Cell Biology, Stem Cells and Development Graduate Program, and Children's Hospital Colorado, University of Colorado Anschutz Medical Campus Aurora, CO 80045, USA

*Author for correspondence (Lee.Niswander@ucdenver.edu)

Biology Open 1, 874–883
doi: 10.1242/bio.20121982
Received 16th May 2012
Accepted 6th June 2012

Summary

Holoprosencephaly is the most common forebrain defect in humans. We describe two novel mouse mutants that display a holoprosencephaly-like phenotype. Both mutations disrupt genes in the glycerophosphatidyl inositol (GPI) biosynthesis pathway: *gonzo* disrupts *Pign* and *beaker* disrupts *Pgap1*. GPI anchors normally target and anchor a diverse group of proteins to lipid raft domains. Mechanistically we show that GPI anchored proteins are mislocalized in GPI biosynthesis mutants. Disruption of the GPI-anchored protein Cripto (mouse) and TDGF1 (human ortholog) have been shown to result in holoprosencephaly, leading to our hypothesis that Cripto is the key GPI anchored protein whose altered function results in an HPE-like phenotype. Cripto is an obligate Nodal co-factor involved in TGFβ signaling, and we show that TGFβ signaling is reduced both *in vitro* and *in vivo*. This work demonstrates the importance of the GPI anchor in normal forebrain development and suggests that GPI biosynthesis genes should be screened for association with human holoprosencephaly.

Key words: Holoprosencephaly (HPE), forebrain, glycerophosphatidyl inositol, GPI, Pign, Pgap1, TGFβ, Cripto, Nodal

Introduction

Holoprosencephaly (HPE) is estimated to occur in 1 in 250 pregnancies but due to prenatal lethality, only 1 in 16,000 babies are born with HPE (Muenke and Beachy, 2000). HPE occurs when the forebrain fails to septate into the two frontal lobes. The spectrum of septal defects that result in HPE are classified as lobar (fully septated, mild), semi-lobar (incompletely septated, moderate), alobar (not septated, severe) and syntelencephaly (posterior frontal lobe and parietal lobe fail to septate). Infants born with HPE, generally representing the mildest spectra, may present with craniofacial defects, hydrocephaly, feeding issues and early mortality.

Environmental and genetic factors contribute to HPE. Environmental causes include maternal diabetes and exposure to alcohol, retinoic acid and cholesterol reducing agents. Large chromosomal defects, such as trisomy 13 account for the majority of HPE cases, but single gene disruptions are also linked to HPE. These single gene mutations segregate into the SHH pathway (SHH, PTCH, GLI2, ZIC2 and DHCR7) and TGFβ pathway (TGIF, FAST1 and TDGF1), but only account for 15–20% of human HPE (Ming and Muenke, 2002). SHH pathway mutations are directly associated with midline defects whereas TGFβ pathway mutants are thought to act upstream of SHH, affecting SHH expression and/or activity in the prechordal plate (Rohr et al., 2001). In mouse, additional TGFβ pathway genes (*Nodal*, *Gdf1*, *Smad2* and *ActRIIA*) have been linked to HPE (Nomura and Li, 1998; Song et al., 1999; Hoodless et al., 2001; Lowe et al., 2001; Rohr et al., 2001; Yamamoto et al., 2001; Andersson et al., 2006) and disruption of both copies of the TGFβ genes often leads to forebrain truncations, rather than classic HPE, due to the requirement for TGFβ signaling in early forebrain initiation steps.

Nodal, a TGFβ ligand, and Cripto, Nodal's obligate co-factor (Gritsman et al., 1999) are both required for specification and localization of the distal visceral endoderm (DVE) and anterior visceral endoderm (AVE) (Varlet et al., 1997; Ding et al., 1998; Mesnard et al., 2006; D'Andrea et al., 2008; Liguori et al., 2008; Takaoka et al., 2011). The AVE is a transient organizing center that initiates forebrain specification in the underlying neuroectoderm. Although DVE progenitors initially require Nodal signaling (Varlet et al., 1997; Mesnard et al., 2006), proper migration of the DVE and AVE is only achieved by antagonism of Nodal and Wnt signaling (Yamamoto et al., 2004; Kimura-Yoshida et al., 2005). Furthermore, the AVE and future forebrain organizing centers induce and then maintain forebrain specification by antagonizing TGFβ and Wnt signaling (Perea-Gomez et al., 2002).

Cripto (the HPE gene TDGF1 in humans) protein is post-translationally modified with a GPI anchor (Minchiotti et al., 2000). This sugar-lipid anchor targets Cripto to the plasma membrane where it binds Nodal to signal in a cell autonomous function (Yan et al., 2002). Cripto's GPI anchor may also be cleaved, releasing Cripto into the extracellular space where it may bind Nodal and signal non-cell autonomously (Yan et al., 2002; Chu et al., 2005; Watanabe et al., 2007).

Here, we describe two novel recessive mutations in mouse, which result in HPE or an anterior truncation phenotype, similar to phenotypes associated with homozygous mutation of TGFβ genes. These mutations disrupt two different enzymes within the GPI biosynthesis pathway. We hypothesize that Cripto is a key GPI-anchored protein, whose lack of a functional GPI anchor results in an HPE-like phenotype. We show that Nodal/Cripto signaling is downregulated both *in vitro* and *in vivo* in the GPI biosynthesis mutants.

Materials and Methods

Mouse strains and genotyping

The *gonzo* (*gnz*) line was derived from a forward genetic screen performed in collaboration with the laboratories of Kathryn Anderson and Elizabeth Lacy and the *beaker* (*bkr*) line was generated from mutagenized males provided by Monica Justice and the screen performed with the lab of Trevor Williams. Both lines were generated on a C57BL/6J genetic background and initially out-crossed to either C3H/HeJ (*gnz*) or 129SI/Sv1mJ (*bkr*) strains. Further analysis of *gnz* and *bkr* was performed in 129SI/Sv1mJ and C57BL/6J backgrounds, respectively. Additional strains used were $Nodal^{LacZ}$ (Collignon et al., 1996), GPI-GFP (Rhee et al., 2006) and Hex-GFP (Rodriguez et al., 2001).

Gonzo was initially mapped between SSLP markers D1MIT136 and D1MIT94. Additional high-resolution markers were generated from NCBI Mouse SNP database (http://www.ncbi.nlm.nih.gov/SNP/MouseSNP.cgi) and Mouse Genome SSR search website (http://danio.mgh.harvard.edu/mouseMarkers/musssr.html). Ultimately, *gnz* was genotyped using ARMS primers: TGCTTTCTTGTTACCTC-CAGCTCACCAG (Pign outer forward), ATGACATCCGTAGGGCCTTTTTC-CTAGAAA (Pign inner A forward), GGAAGATCTTAACAATCCCAGAGCA-AAGGA (Pign inner T reverse) and GCACCTGCCATCTCCAAATTTTTGGT (Pign outer reverse) (Ye et al., 2001). *Beaker* was initially mapped between D1MIT123 and D1MIT303 and ultimately genotyped using SNP analysis with primers: CCGTAGACCATTGCATTCAGCCAT (Pgap1 snpF), GCAATCCCTT-CCAAATCACAAAGC (Pgap1 snpR), and TCCTTCCCACAAATACTTGGA-CAGG (Pgap1 snp probe). $Pign^{gnz}$ (renamed $Pign^{m1Nisw/J}$) and $Pgap^{bkr}$ (renamed $Pgap^{1m1Nisw/J}$) have been deposited and are available from Jackson Laboratories. GFP strains were genotyped using primers oIMR0872 and oIMR1416 and LacZ identified using oIMR0039 and oIMR0040 (Jackson Labs).

Mouse embryo fibroblasts (MEFs), cell culture and immunodetection

MEFs were prepared from E13.5 embryos. Embryos were dissected in DMEM (Gibco), eviscerated, decapitated and minced with a sterile blade, followed by trypsination for up to 30 min. MEFs were maintained in 10% FBS (Gibco) in DMEM with Penicillin/Streptomycin (Gibco).

For immunostaining, 12,000 MEFS ($Pign^{+/+}$ or $Pign^{gnz/gnz}$) were plated on coverslips in 24-well plates (Falcon). MEFs were grown in 10% FBS in DMEM, fixed in 4% paraformaldehyde then analyzed by immunodetection for βCOP (GeneTex, Inc).

For *in vitro* Nodal/Cripto signaling assays, 100,000 MEFs ($Pign^{+/+}$, $Pign^{gnz/gnz}$, $Pgap1^{+/+}$ or $Pgap1^{bkr/bkr}$) were plated in 6-well plates in 10% FBS in DMEM. Cells were transfected with pCDNA3-HA-Cripto (Yan et al., 2002) or pCDNA3.1 (Invitrogen) using Lipofectamine 2000 Transfection Reagent (Invitrogen) for 4 hours, then medium changed to DMEM (no serum) overnight. MEFs were treated with 250 ng/ml recombinant Nodal protein (R&D Systems) or vehicle for 1 hour; protein extracts were prepared and separated by SDS-PAGE.

For detection of Cripto from conditioned medium, 100,000 MEFs ($Pign^{+/+}$, $Pign^{gnz/gnz}$, $Pgap1^{+/+}$ or $Pgap1^{bkr/bkr}$) were plated in 6-well plates in 10% FBS in DMEM. Medium was changed to 2 ml DMEM (no serum) overnight. Conditioned medium was spun down to remove cellular debris, 1.8 ml conditioned medium was pre-cleared with 50 µl Protein A/G agarose (Santa Cruz) for 4 hours at 4℃, then 0.4 µg/ml anti-Cripto antibody was added and complexes were rocked 1 hour at 4℃. 50 µl Protein A/G agarose was added and complexes were rocked overnight at 4℃. Complexes were spun down and washed twice with 50 mM Tris (pH 7.5), 150 mM NaCl, 1% NP-40, 0.5% sodium deoxycholate, and protease inhibitors, then twice with 50 mM Tris (pH 7.5), 500 mM NaCl, 0.1% NP-40 and 0.05% sodium deoxycholate and then twice with 50 mM Tris (pH 7.5), 0.1% NP-40 and 0.05% sodium deoxycholate. For each wash, tubes were rotated for 20 minutes at 4℃ followed by brief centrifugation to pellet the Protein A/G agarose and bound complexes. 1× Laemmli buffer was added and immunoprecipitated conditioned medium was boiled for 10 min prior to analysis by SDS-PAGE.

Western blots were performed with Smad2, phosphor-Smad2 (Cell Signaling 3122 and 3101) and Cripto (R&D Systems AF1538) antibodies. Blots were performed in triplicate and quantitated on Bio-Rad gel documentation system.

Real time polymerase chain reaction

Total RNA was extracted from E7.5 embryos using an RNeasy Micro Kit (QIAgen). Six wildtype littermates and six $Pign^{gnz/gnz}$ or $Pgap1^{bkr/bkr}$ embryos were used for real time PCR with the Mouse TGFβ BMP Signaling Pathway RT^2 Profiler PCR Array (SABiosciences) using 200 ng of reverse transcribed RNA as template.

Results

Characterization of the ENU-derived *Gonzo* mutant mouse line

To identify novel genes important for normal forebrain development, we employed an ENU mutagenesis screen in mice. Briefly, mutagenized C57BL/6J (C57) males were out-crossed to C3H/HeJ (C3H) females to generate founder males. Founder males were further out-crossed, and then mated to their daughters to produce litters that would include homozygous mutant embryos. From this screen, we identified mutant embryos with forebrain truncations or an HPE-like phenotype. Due to the presence of a large proboscis that dominated the craniofacial region we named this line *gonzo (gnz)*.

In the C3H background, *gnz* mutant embryos show three different phenotypes: dysmorphic eyes (n=14/39 embryos) (supplementary material Fig. S1A,B), gastrulation defects (9/39) (supplementary material Fig. S1I,J), and an HPE-like phenotype in which mutant embryos either display midline defects (n=2/39) (supplementary material Fig. S1K,L) or anterior truncations (n=14/39) (supplementary material Fig. S1E,F; Fig. 1A,D). When out-crossed into 129S1/Sv1mJ (129S1) background, *gnz* mutant embryos largely present with anterior truncations. While the C3H strain was used for mutation mapping, the 129S1 strain was used for the majority of results and figures presented here.

A typical *gnz* mutant at embryonic day 18.5 (E18.5) shows midbrain/forebrain truncation and a large proboscis (Fig. 1D). To identify the rostral-caudal position of the truncation, bone and cartilage staining was performed (Fig. 1B,C,E,F). In *gnz* mutant embryos, bone and cartilage structures anterior to the interparietal (ip) element remain symmetrical yet are grossly misshapen. The ip, while recognizable, is tiny and misshapen. The tectum synoticum (tso) is largely intact, but narrower at the anterior midline. Occipital elements at the base of the skull are also dysmorphic. The supraoccipital (so) and exoccipital (eo) elements are fused and the supraoccipital is present as two lateral bony elements instead of the normal rod-like shape. The basioccipital (bo) element appears normal in *gnz* mutants.

In addition to the anterior truncation, *gnz* mutant embryos are smaller than wildtype littermates (supplementary material Fig. S2A,B). Comparison of the lengths of femurs and humeri from five mutant and wildtype E18.5 embryos (supplementary material Fig. S2C,D,I) reveal a statistically significant shortening of the femur (by 11%, P value=0.04; unpaired, 2-tailed Student's t-test) but not the humerus (P value=0.24) in *gnz* mutant embryos.

Gnz mutation disrupts *Pign*, encoding a glycerophosphatidyl inositol biosynthesis enzyme

We mapped the *gnz* mutation to a 5 Mb region on mouse chromosome 1 using Simple Sequence Length Polymorphisms (SSLPs) and Single Nucleotide Polymorphisms (SNPs) that differ between the mutagenized C57 DNA and the out-crossed C3H DNA (Fig. 1G) (between rs3654716 and rs6307336). This gene sparse region contained seven known or predicted genes. Sequencing of these seven genes revealed a single base substitution (T to A) in the splice donor region of intron 23 of the *Phosphatidylinositol-glycan*

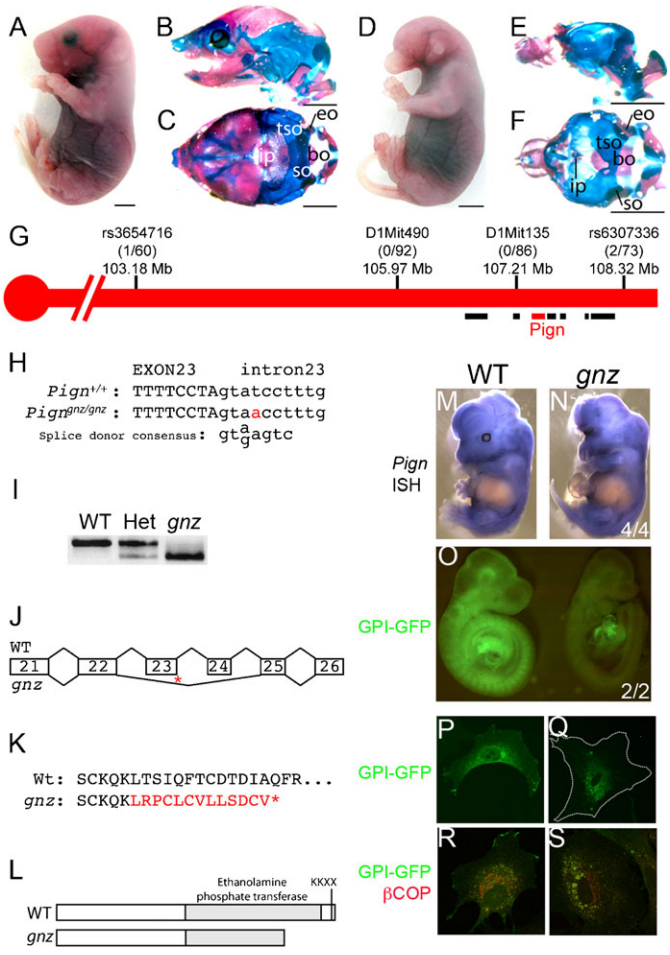

Fig. 1. Mutation of the glycerophosphatidyl inositol biosynthesis enzyme Pign leads to anterior truncations in *Gonzo* mutant embryos. Wildtype (**A–C**) and *gnz* (**D–F**) mutant E18.5 embryos with lateral (B,E) and top (C,F) views of skull stained for bone (red) and cartilage (blue). Exoccipital (eo), supraoccipital (so), basioccipital (bo), tectum synoticum (tso) and interparietal (ip) elements are indicated. Critical 5.14 Mb region of chromosome 1 that the *gnz* mutation mapped to by meiotic recombination (**G**). Recombinants are shown in parentheses divided by number of recombination opportunities. SNP and SSLP markers and known or predicted genes (horizontal bars) are indicated. There is a T to A transversion in the splice donor of *Pign's* intron 23 (**H**) that causes skipping of exons 23 and 24 (**J**) as shown by PCR amplification of wildtype (WT), heterozygote (Het) and *gnz* mutant cDNA (**I**). Mis-splicing of exon 22 to 25 results in a frame shift and premature stop codon within 13 amino acids from the mutation (**K**) leading to truncation and partial loss of the catalytic domain and KKXX ER-retention motif (**L**). *Pign* mRNA detected by whole mount *in situ* hybridization in E14.5 wildtype (**M**) and $Pign^{gnz/gnz}$ mutant (**N**) embryos, showing ubiquitous and stable expression in *gnz* mutants. GFP fluorescence was detected in E13.5 $Pign^{+/+}$; $Tg^{GPI\text{-}GFP}$ (**O** -left) but was greatly reduced in $Pign^{gnz/gnz}$; $Tg^{GPI\text{-}GFP}$ (O -right) embryos and MEFs (**P–S**; P and R are $Pign^{+/+}$; $Tg^{GPI\text{-}GFP}$ MEFs and Q and S are $Pign^{gnz/gnz}$; $Tg^{GPI\text{-}GFP}$ MEFs). Panels R and S were immunostained for the Golgi marker βCOP (red). See also supplementary material Fig. S1 for mutant phenotypes. Ratios in lower right of panels N,O and subsequent figures indicate number of similar phenotypes observed out of number of mutant embryos analyzed. Scale bars (A–F)=2 mm.

biosynthesis class N (*Pign*) gene (Fig. 1H). *Pign* encodes one of 27 endoplasmic reticulum (ER) localized enzymes that are required to make GPI anchors (Kinoshita et al., 2008). Specifically, Pign adds phosphoethanolamine to the first mannose in the GPI anchor (supplementary material Fig. S3) (Gaynor et al., 1999; Hong et al., 1999).

While the T to A transversion in intron 23 of *Pign* would be predicted to create a more optimal splice consensus site, splicing is nevertheless disrupted in *gonzo* mutant embryos. PCR amplification of *gnz* HPE-like mutant cDNA yielded a shorter amplicon than wildtype, and cDNA from a heterozygous embryo yielded both products (Fig. 1I). Sequencing of the *gnz* mutant amplicon revealed that both exons 23 and 24 were excluded from the *Pign* transcript (Fig. 1J). To determine whether nonsense-mediated decay may contribute to the phenotype, the expression level and localization of *Pign* RNA was analyzed by semi-quantitative PCR and whole mount *in situ* hybridization of E14.5 embryos. There were no significant changes in expression level (data not shown) or localization (Fig. 1M,N) of *Pign* between *gnz* mutants and wildtype littermates.

Conceptual translation of the $Pign^{gnz}$ transcript predicts a frameshift that adds 13 divergent amino acids followed by a stop codon (Fig. 1K), causing early termination and loss of the carboxy-terminal 170 amino acids of the 931 amino acid protein (Fig. 1L). The truncated C-terminus includes part of the ethanolamine phosphate transferase domain as well as a KKXX ER retention motif (Vincent et al., 1998), suggesting that the truncated Pign protein lacks catalytic activity and is mislocalized.

Gnz mutant embryos show mislocalized GPI anchored proteins

Pign mutants have been described in yeast and mouse cell lines (Gaynor et al., 1999; Hong et al., 1999). These mutated cells show mislocalization of GPI-anchored proteins (GPI-APs). To determine whether GPI-APs are mislocalized in *gnz* mutants, the *gnz* line was crossed into a transgenic mouse line in which GFP is targeted to the membrane by a GPI linkage (Rhee et al., 2006). While GPI-GFP is highly expressed in wildtype E12.5 embryos, *gnz* mutant embryos show a dramatic reduction in GPI-GFP fluorescence (Fig. 1O). The subcellular distribution of GPI-GFP in mouse embryonic fibroblasts (MEFs) from E12.5 wildtype embryos show GFP localization in the plasma membrane, whereas *gnz* mutant MEFs show only internal localization of GFP in numerous apparently membrane-bound structures surrounding the nucleus (Fig. 1P,Q). These structures are consistent with those seen in budding yeast with a mutation in the *Pign* ortholog *Mcd4* (Gaynor et al., 1999). Immunostaining with βCOP, a marker of the Golgi compartment, reveals these structures express Golgi markers (Fig. 1R,S).

Beaker mutant embryos display anterior truncations

A second ENU-derived mouse line that displays an HPE-like phenotype was isolated from an independent screen. Dependent on the background strain, homozygous mutant embryos from the *beaker* mouse line also display a range of phenotypes – normal appearance in 129S1, anterior truncations in C57 (Fig. 2B,D), and holoprosencephaly (Fig. 2A,C) and/or eye defects (supplementary material Fig. S1C,D) in mixed 129S1/C57 strains. Further analysis of the *bkr* line was performed in the C57 background, which gave the fully penetrant phenotype shown in Fig. 2D.

Bone and cartilage staining of wildtype and *bkr* mutant embryos at E18.5 (Fig. 2E–H) reveal the interparietal element is dysmorphic and not ossified and the tectum synoticum is present as two lateral elements that do not traverse the midline. All elements rostral to these are largely absent. The supraoccipital and exoccipital elements are correctly positioned, but not ossified, whereas the basioccipital element is absent. *Bkr*

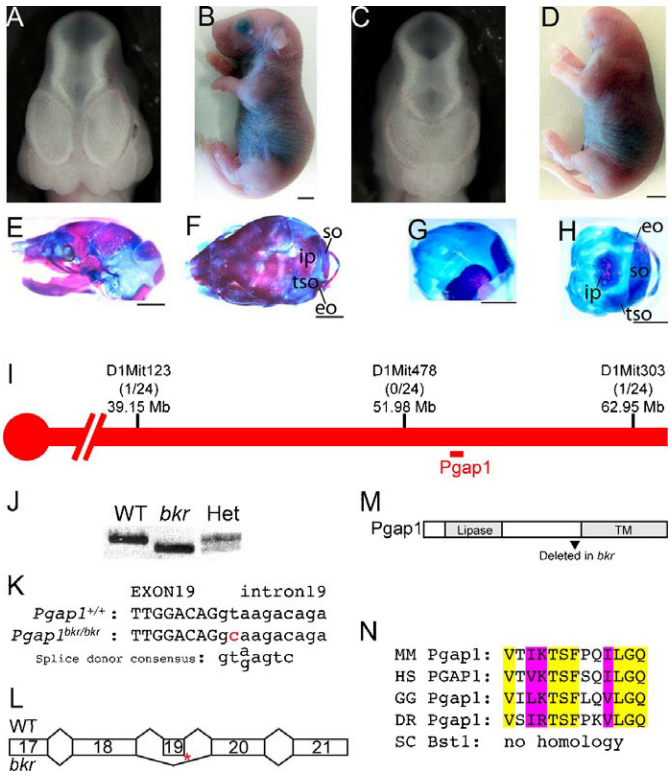

Fig. 2. Mutation of the glycerophosphatidyl inositol deacylase *Pgap1* results in anterior truncations in *Bkr* mutant embryos. Wildtype (**A**) and *bkr* mutant (**C**) E11.5 embryos reveal HPE in *bkr* mutants. Wildtype (**B**,**E**,**F**) and *bkr* mutant (**D**,**G**,**H**) E18.5 embryos with lateral (E,G) and top (F,H) views of skull stained for bone and cartilage. Abbreviations as in Fig. 1. (**I**) 23.8 Mb region of chromosome 1 that the *bkr* mutation mapped to by meiotic recombination. The *Pgap1* gene (red horizontal bar) is shown but not the other 144 genes in this interval. There is a T to C transition in the splice donor of intron 19 of *Pgap1* (**K**) that causes skipping of exon 19 (**L**) as shown by PCR of wildtype (WT), heterozygote (het) and *bkr* mutant cDNA (**J**) and sequencing. Mis-splicing of exon 18 to 20 results in an in-frame deletion of 13 amino acids that are conserved (identical amino acids highlighted in yellow, conserved in pink) among human (HS), chick (GG) and zebrafish (DR) *Pgap1* orthologs (**N**). These deleted amino acids lie outside of domains of known function (**M**). Scale bars (A–H)=2 mm.

mutant embryos are smaller than wildtype littermates with significant shortening of the femur (10.4%, P value=0.01) and humerus (5.7%, P value=0.02) (supplementary material Fig. S2E–H,J).

Bkr mutation disrupts *Pgap1*, encoding a second glycerophosphatidyl inositol biosynthesis enzyme

We mapped the *bkr* mutation to a 24 Mb region, containing 145 predicted genes, on mouse chromosome 1 (Fig. 2I). Based on similarity to the *gnz* phenotype and discovery of the *Pign* mutation, we cross-referenced these genes with known GPI biosynthesis genes and found that *Post-GPI Attachment to Proteins factor 1* (*Pgap1*) lies within this region. Pgap1 is an ER localized deacylase that removes an acyl group from the GPI anchor after covalent attachment to its target proteins (supplementary material Fig. S3). Deacylation of GPI anchored proteins allows efficient loading into CopII coated vesicles and transport to the Golgi (Tanaka et al., 2004).

PCR amplification of *Pgap1* revealed a size difference between wildtype and *bkr* mutant cDNAs in PCR products that span exon 19 (Fig. 2J). Sequencing of genomic DNA at the exon/intron borders of exon 19 revealed a base substitution (T to C) in the splice donor of intron 19 (Fig. 2K) and sequencing of cDNA showed skipping of exon 19 in *bkr* mRNA (Fig. 2L). Exon 19 is 39 nucleotides, and its exclusion is predicted to result in an in-frame deletion of 13 amino acids. While these 13 amino acids do not correspond to a domain of known function, these residues are well conserved between human, mouse, chick and zebrafish, though not in S. cerevisiae (Fig. 2M,N). The $Pign^{gnz}$ (renamed $Pign^{m1Nisw/J}$) and $Pgap^{bkr}$ (renamed $Pgap^{1m1Nisw/J}$) mouse lines are available from Jackson Laboratories.

Forebrain patterning defect in *Pign* and *Pgap1* mutant mouse embryos

Apart from anterior truncations, *gnz* (in 129S1 background) and *bkr* mutant embryos display relatively normal development, which is remarkable as there are more than one hundred GPI anchored proteins. Consistent with normal trunk development, the trunk mesoderm marker *Brachyury* is expressed normally in E6.5 and E7.5 *gnz* and *bkr* mutants (Fig. 3A–D).

The dysmorphic occipital elements in both *gnz* and *bkr* mutants prompted investigation of markers of hindbrain development. *Krox20* expression in rhombomeres 3 and 5 (r3 and r5) in headfold-stage embryos (E8.5) is altered in these mutants (Fig. 3E–H). In *gnz* mutants, *Krox20* expression in r3 is reduced, and expanded in r5. In *bkr* mutants, *Krox20* expression is normal in r3, but reduced in r5. This implicates GPI biosynthesis as being required for normal hindbrain development, yet this may be a downstream consequence of the lack of anterior tissues.

We next investigated the expression of genes involved in forebrain patterning and/or associated with HPE. In E9.5

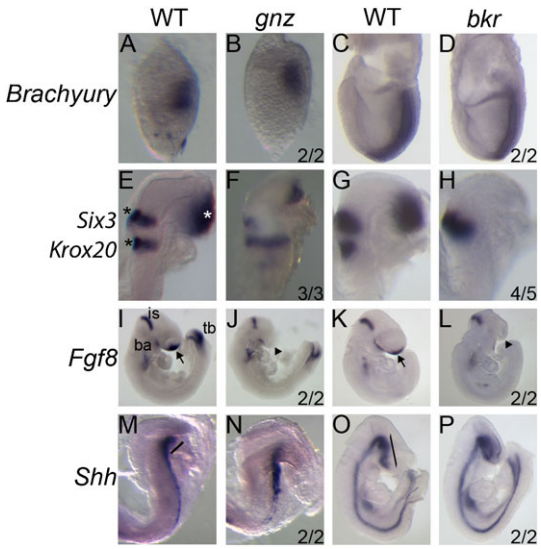

Fig. 3. Forebrain patterning markers are misexpressed in both *Gnz* and *Bkr* mutants. *Gnz* mutant embryos (**B**,**F**,**J**,**N**) and wildtype littermates (**A**,**E**,**I**,**M**) and *bkr* mutant embryos (**D**,**H**,**L**,**P**) and their wildtype littermates (**C**,**G**,**K**,**O**) were analyzed by whole mount RNA *in situ* hybridization for *Brachyury* (A–D), *Six3* and *Krox20* (E–H), *Fgf8* (I–L) and *Shh* (M–P). Embryos were at E6.5 (A,B), E7.5 (C,D), E8.5 (E–H,M,N) and E9.5 (I–L,O,P). Black and white asterisks in E denote *Krox20* and *Six3* expression, respectively. Abbreviations: is=isthmus; ba=branchial arches; tb=tailbud. Arrows and arrowheads denote presence or absence, respectively of *Fgf8* expression in the ANR (I–L). Black bars mark prechordal plate (M,O).

embryos, the anterior neural ridge (ANR) acts as a forebrain "organizing center" by secreting factors necessary to maintain forebrain specification. *Fgf8* is expressed in the ANR, isthmus (midbrain-hindbrain boundary), pharyngeal arches and tail bud. *Fgf8* expression in *gnz* and *bkr* mutants is normal, except in the ANR, where it is not expressed (Fig. 3I–L); lack of *Fgf8* expression likely reflects that the ANR fails to develop and implicates an earlier requirement of GPI biosynthesis in forebrain specification.

Six3 is an earlier anterior forebrain marker. The *Six3* expression domain was both reduced in size and level of expression in E8.5 *gnz* mutants, and severely reduced or absent in *bkr* mutants (Fig. 3E–H). Six3 function is required for forebrain development (Lagutin et al., 2003) and mutation of human SIX3 causes HPE; hence decreased *Six3* expression is consistent with forebrain defects. The relative decrease in *Six3* expression in *bkr* versus *gnz* mutant embryos also correlates with the extent of anterior truncation.

Shh is expressed in the prechordal plate underlying the anterior neural tube and is required for septation of the future forebrain into left and right hemispheres. Mutations in human SHH and its signaling pathway are linked to HPE. *Shh* expression is decreased in the prechordal plate of both E8.5 *gnz* and E9.5 *bkr* mutant embryos (Fig. 3M–P). The disrupted expression patterns of *Fgf8*, *Six3* and *Shh* indicate an early defect in forebrain specification.

Early forebrain organizing centers are disrupted in *gnz* and *bkr* mutant embryos

Otx2, which is expressed in the anterior definitive endoderm (ADE) and underlying anterior neuroectoderm in gastrulation stage (E7.5) embryos, is required for forebrain specification. The node-derived ADE migrates anteriorly and acts as an organizing center to maintain forebrain development in the neuroectoderm. *Otx2* expressing cells are mislocalized at the distal tip of E7.5 *gnz* mutant embryos whereas E7.75 *bkr* mutant embryos display proper localization of *Otx2* expression albeit at a reduced level (Fig. 4A–D). Alteration in *Otx2* localization (*gnz*) and expression (*bkr*) suggests that ADE cellular migration or specification might be disrupted in GPI biosynthesis mutants.

To examine ADE migration and specification, we crossed *gnz* and *bkr* lines into Hex-GFP transgenic mouse line (Rodriguez et al., 2001; Stuckey et al., 2011) to visualize *Hex* expression and ADE localization. Both *gnz* and *bkr* E7.5 embryos showed a modest displacement of the ADE towards the distal tip compared to wildtype embryos (Fig. 4E–H). While defects in ADE migration can cause anterior truncation phenotypes, examination of Hex-GFP at an earlier stage allows visualization of both the DVE and AVE, two molecularly distinct, migratory groups of cells that contribute to forebrain specification. The DVE migrates towards the presumptive anterior pole at ~E5.5, 'paving the road' for subsequent AVE migration (Takaoka et al., 2011). At the anterior pole, the AVE initiates forebrain specification then is displaced and *Hex* expression is downregulated (Rodriguez et al., 2001). Hex-GFP fluorescence (which does not distinguish the DVE from the AVE) in *gnz* and *bkr* E6.5 embryos reveals aberrant DVE/AVE localization (Fig. 4I–L). *Gnz* mutants show DVE/AVE displacement at the distal tip. However, *bkr* mutant embryos have promiscuous GFP expression throughout the visceral endoderm, reminiscent of cultured embryos in which the extraembryonic ectoderm has been removed (Rodriguez et al., 2005). Together this indicates that GPI biosynthesis proteins are required to properly initiate forebrain development. Moreover, this allowed us to make some predictions as to the identity of the GPI-AP(s) that may be altered resulting in the HPE-like phenotype based on involvement in AVE specification and migration, and perhaps communication with the extraembryonic ectoderm.

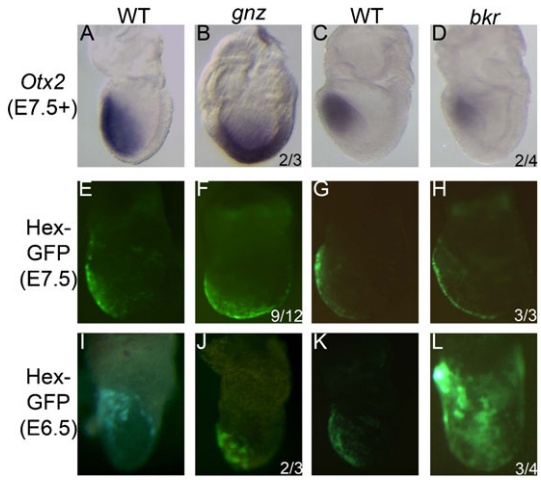

Fig. 4. Forebrain organizing centers are mislocalized in both *Gnz* and *Bkr* mutants. E7.5 wildtype (**A**) and *gnz* mutant (**B**) littermates and E7.75 wildtype (**C**) and *bkr* mutant (**D**) littermates were analyzed by whole mount RNA *in situ* hybridization for *Otx2*. *Gnz* mutant embryos (**F**,**J**) and wildtype littermates (**E**,**I**) and *bkr* mutant (**H**,**L**) and wildtype littermates (**G**,**K**), all containing *Hex*-GFP transgene were analyzed by GFP fluorescence. *Hex*-GFP fluorescence marked the ADE in E7.5 embryos (E–H) and DVE/AVE in E6.5 embryos (I–L).

The Nodal/Cripto signaling pathway is defective in *Pign* and *Pgap1* deficient cell lines

Given the migration and specification defects of the AVE in E6.5 *gnz* and *bkr* mutant embryos, we hypothesized that Cripto is the GPI anchored protein whose GPI deficiency leads to the HPE-like phenotype. We analyzed Nodal/Cripto signaling in wildtype and mutant MEFs by phosphorylation of Smad2 (Watanabe et al., 2007). In the absence of exogenous Nodal stimulation, wildtype, $Pign^{gnz}$ and $Pgap1^{bkr}$ MEFs, which express endogenous Cripto, have negligible phospho-Smad2 and this is not significantly increased by Cripto overexpression (transfection of HA-tagged Cripto expression vector compared to empty vector, mock stimulated cells) (Fig. 5A–C). Upon Nodal stimulation in wildtype cells, there was a 16-fold increase of phospho-Smad2 in empty vector transfected cells (P value=0.003) and 35-fold increase with Cripto overexpression (Fig. 5A–C) (P value=0.007). In contrast, Nodal stimulation of *gnz* or *bkr* MEFs, in the presence or absence of Cripto overexpression, showed a significantly lower response (Fig. 5A–C) (approximately 3-fold lower for both *gnz* [P value=0.03 with or without Cripto] and *bkr* [P value=0.04 without Cripto, and 0.02 with Cripto]). Thus, GPI biosynthetic activity is required for efficient Nodal/Cripto signaling.

In $Pign^{gnz}$ and $Pgap1^{bkr}$ mutant MEFs, there was some response to Nodal stimulation, suggesting that endogenous or transfected Cripto retained some signaling activity. Cripto can function non-cell autonomously via enzymatic or genetic removal of its GPI anchor (Zhang et al., 1998; Yan et al., 2002; Watanabe et al., 2007), demonstrating that secreted Cripto retains biological activity. Furthermore, secretion of GPI

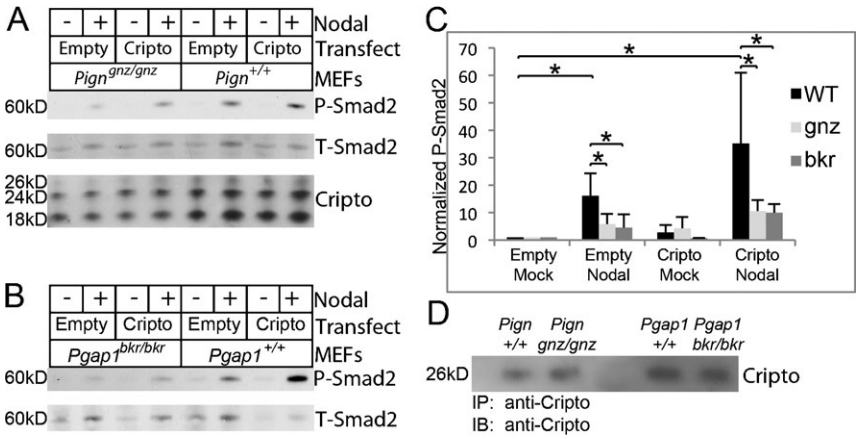

Fig. 5. Cripto/Nodal signaling is defective in MEFs derived from *Gnz* and *Bkr* embryos. Wildtype and $Pign^{gnz/gnz}$ MEFs (**A**) or wildtype and $Pgap1^{bkr/bkr}$ MEFs (**B**) were transfected with HA-Cripto-pcDNA3 expression vector (Cripto) or pcDNA3 vector (Empty), serum starved, then treated with 250 ng/ml recombinant Nodal protein (+) or vehicle (−) for 1 hour. Whole cell extract was separated by SDS-PAGE, and phosphorylated (P-Smad2) and total Smad2 (T-Smad2) and Cripto proteins detected by western blot. (**C**) Quantification of at least three independent Cripto/Nodal signaling experiments. * represents statistical significance (P value<0.05) by Student's T-test. (**D**) Endogenous Cripto protein was immunoprecipitated from serum-free conditioned medium overlying $Pign^{+/+}$, $Pign^{gnz/gnz}$, $Pgap1^{+/+}$ and $Pgap1^{bkr/bkr}$ MEFs, separated by SDS-PAGE and detected by western blot.

anchored proteins was detected in *Mcd4* (*Pign* ortholog) mutant budding yeast (Gaynor et al., 1999). Cripto overexpression, while resulting in increased Smad2 phosphorylation, has no effect on intracellular Cripto protein levels (Fig. 5A) suggesting that some Cripto protein could be secreted and act in a non-autonomous manner. To test this we immunoprecipitated endogenous secreted Cripto from conditioned medium from wildtype and mutant MEFs followed by western blot detection (Fig. 5D). Although not quantitative, this showed Cripto protein in the medium, consistent with reduced but not absent Smad2 phosphorylation in both *gnz* and *bkr* MEFs.

TGFβ responsive genes are downregulated in *gnz* and *bkr* mutant embryos

As another measure of Cripto/Nodal activity we determined the expression of TGFβ target genes by real time PCR using TGFβ/BMP pathway arrays and E7.5 RNA from mutants compared to wildtype littermates, as the two lines are in different background strains. Seven of 22 TGFβ responsive genes were significantly (P value<0.05) downregulated in *bkr* mutants and 3 of 22 TGFβ responsive genes were significantly downregulated in *gnz* mutants as compared to wildtype littermates (Table 1). *Collagen, type1 alpha-2* (*Col1a2*) and *Interleukin6* (*Il6*) were downregulated in both *gnz* and *bkr* mutants. BMP signaling is not dependent on Cripto activity, so BMP responsive genes can serve as a negative control since these genes are predicted to be unchanged in GPI biosynthesis mutants. Correspondingly, only the BMP responsive gene *Stat1* showed significantly altered expression, and only in *bkr* mutant embryos. The array also includes other genes in the TGFβ/BMP signaling pathway, many of which display significantly altered expression levels in the GPI biosynthesis mutants.

All TGFβ responsive genes that are significantly altered in *gnz* and *bkr* mutant embryos are downregulated. In contrast, 41% of the other genes in the TGFβ/BMP signaling pathway that are significantly altered are upregulated (9 out of 22). Together these data indicate that TGFβ signaling is defective in E7.5 *gnz* and *bkr* mutant embryos and corroborates the *in vitro* data showing that Nodal/Cripto signaling is defective in GPI deficient cell lines.

Discussion

GPI biosynthesis mutants and HPE

Herein we describe novel mutations in two GPI biosynthesis genes that result in an HPE-like phenotype in mice. In humans, mutations in the GPI biosynthesis pathway have not been implicated in HPE, although mutations are associated with other diseases, including Paroxysmal Nocturnal Hemoglobinuria (PIGA somatic mutation) and Inherited GPI Deficiency (hypomorphic mutation in the PIGM promoter). A human PIGN mutation (R709Q) has been linked to an autosomal recessive syndrome presenting with developmental delay, dysmorphic facies, seizures and severe neurological impairment (Maydan et al., 2011). It is interesting to speculate that different PIGN alleles may yield a range of phenotypes from neurological defects to structural, HPE-like defects. Our identification of mutations in two GPI biosynthesis enzymes, which result in HPE-like phenotypes in mice, greatly expands an understanding of the genetic causes of HPE and suggests that this entire enzymatic pathway of 27 genes represent novel candidate genes for analysis in human HPE or related disorders.

Complete loss of GPI anchors is embryonic lethal in mice, as demonstrated by knockout of *Piga*, a critical and early GPI biosynthesis enzyme (Kawagoe et al., 1996; Tremml et al., 1999). Conditional knockout of *Piga* in chondrocytes leads to mice with shortened bones, similar to that in $Pign^{gnz}$ and $Pgap1^{bkr}$ mutants. Previous mutant alleles of *Pgap1* show a similar forebrain truncation phenotype as $Pign^{gnz}$ and $Pgap1^{bkr}$ mutant embryos, though the authors labeled it as otocephaly, as well as growth retardation, mislocalization of GPI-APs and a sperm activation defect. (Juriloff et al., 1985; Zoltewicz et al., 1999; Ueda et al., 2007; Zoltewicz et al., 2009). Both $Pign^{gnz}$ and $Pgap1^{bkr}$ embryos are growth retarded and GPI-GFP is mislocalized in $Pign^{gnz}$ mutant embryos. We also observed a genetic interaction between *Pign* and *Nodal* suggestive of a sperm defect. In a genetic cross between mice harboring a single *Nodal* null allele (*Nodal-LacZ*) and a single $Pign^{gnz}$ allele (i.e. $Nodal^{+/LacZ} \times Pign^{+/gnz}$ or $Nodal^{+/LacZ}$; $Pign^{+/gnz} \times$ wildtype) we observed a less than expected proportion of *Nodal-LacZ*:*gnz* trans-heterozygotes at E7.5 (18.1%, $n=115$; P value>0.05 using χ^2 test). Moreover, skewing of the expected ratio only occurred when the father was a trans-heterozygote mated to a wildtype female (14.8%, $n=216$, P value$=0.05$). In all other combinatorial matings, the number of trans-heterozygotes was as expected (23.1%, $n=199$). The *Pign* and *Nodal* genetic interaction was statistically significant, although it addressed viability or perhaps sperm fitness, not forebrain development. The *Pign* and *Nodal* genetic interaction does, however, indicate a genetic link between GPI biosynthesis and TGFβ signaling.

Table 1. Real-time PCR results for TGFβ signaling genes indicate defective TGFβ responses in *Pign*^{gnz} and *Pgap1*^{bkr} embryos. Shown are statistically significant changes in expression levels of genes on the Mouse TGFβ BMP Signaling Pathway RT^2 Profiler PCR Array. Relative expression (Relative Expr.) ± standard error is shown from comparison between E7.5 *Pign*^{gnz} and *Pgap1*^{bkr} homozygous mutants and their respective wildtype littermates (C57BL/6J for *bkr* line and 129S1/Sv1mJ for *gnz*). Data were generated using six embryos of each genotype and discarding the single largest outlier for all genes.

	bkr vs. wildtype		*gnz* vs. wildtype	
Gene Symbol	Relative Expr.	p-value	Relative Expr.	p-value
TGFβ Responsive Genes				
Col1a2	0.57±0.15	0.015	0.26±0.25	0.022
Igf1			0.10±0.10	0.007
Igfbp3	0.36±0.22	0.016		
Il6	0.48±0.18	0.006	0.48±0.12	0.003
Junb	0.69±0.21	0.037		
Pdgfb	0.76±0.09	0.001		
Serpine1	0.42±0.24	0.013		
Tgfbi	0.51±0.28	0.049		
BMP Responsive Genes				
Stat1	0.60±0.19	0.008		
Other TGFβ Superfamily Genes				
Acvrl1	1.36±0.35	0.043		
Amh			0.57±0.16	0.012
Amhr2	0.56±0.21	0.015		
Bmp1	0.59±0.20	0.009		
Bmp7	1.23±0.20	0.037		
Bmper			1.37±0.31	0.038
Chrd	0.65±0.20	0.017		
Fst	0.71±0.18	0.037		
Gdf2	3.35±1.72	0.004	0.54±0.15	0.007
Lefty1	0.43±0.31	0.045		
Ltbp4	0.64±0.20	0.020		
Nbl1			0.22±0.22	0.028
Nog	0.35±0.19	0.026		
Nr0b1	0.35±0.14	0.001		
Runx1	0.65±0.21	0.037		
Smad2			1.39±0.37	0.048
Tgfbr1	1.20±0.15	0.021		

GPI anchored proteins and HPE

Here we sought to identify the key GPI-AP(s) that Pign and Pgap1 act through to regulate normal forebrain development. In a previous report of a *Pgap1* mutant allele, Zoltewicz et al. demonstrated that Wnts are modified with a GPI-like anchor and that midbrain Wnt activation is slightly premature (E8.0 vs. E8.2) (Zoltewicz et al., 2009). The importance of Wnt signaling in forebrain specification has been shown in mice with mutation of *Apc* (Chazaud and Rossant, 2006) or *Dikkopf1* (Mukhopadhyay et al., 2001). Zoltewicz et al. surmised that premature Wnt activation was responsible for otocephaly (Zoltewicz et al., 2009). Our data establish a much earlier origin (E6.5) for the forebrain defect, so it is possible that altered Wnt expression is downstream of an earlier disruption in forebrain development. Although we did not detect a change in Wnt signaling using the Top-Gal Wnt reporter strain, further study is needed to determine whether Wnt signaling is also affected at this early stage in *Pign*^{gnz} and *Pgap1*^{bkr} mutants, as Wnt signaling, in conjunction with TGFβ is important for AVE formation and migration and for forebrain specification.

Gas1 is a GPI-AP that binds Shh and modulates Shh activity, and has been described as a modulator of HPE. *Gas1*$^{-/-}$ mouse embryos present with small eyes and reduced body size (Allen et al., 2007), reminiscent of some *gnz* mutants in C3H/HeJ background (supplementary material Fig. S1A,B). It will be of interest to determine whether GPI disruption targets both the Shh and TGFβ pathways in HPE etiology. It is also interesting to speculate whether another GPI-AP, Glypican 4, is in part responsible for gastrulation defects in some *gnz* C3H/HeJ mutants. Glypican 4 mediates non-canonical Wnt signaling, and the zebrafish mutant Knypek fails to gastrulate due to aberrant cell polarity and disrupted convergent extension (Topczewski et al., 2001). *Cripto* nulls also fail to undergo gastrulation (Ding et al., 1998), so it may be difficult to isolate the contribution of these two genes in gastrulation.

The GPI-anchored Cripto-related protein Cryptic may also contribute to the HPE-like phenotype in GPI biosynthesis mutants. Cryptic expression overlaps Nodal in the DVE, and these two proteins specify the AVE (Chu and Shen, 2010). *Pgap1*^{bkr} mutants might be candidates for altered Cryptic/Nodal signaling, as Hex-GFP is ectopically expressed throughout the visceral endoderm.

The following evidence supports our hypothesis that Cripto is at least one of the key GPI anchored proteins that juxtaposes GPI biosynthesis and forebrain specification: 1. *Pign* and *Pgap1* mutations result in anterior truncations or HPE-like phenotype; *Cripto* hypomorphic mutations in mouse (Chu et al., 2005), Oep mutations in zebrafish (Gritsman et al., 1999) and TDGF1 mutations in humans (de la Cruz et al., 2002) cause HPE. 2. *Pign* and *Pgap1* mutations result in mislocalization (secretion and/or

internalization) of GPI-anchored proteins; Cripto is a GPI anchored protein (Minchiotti et al., 2000), and its GPI anchor is critical for its function (Watanabe et al., 2007). 3. *Pign* and *Pgap1* mutants show defective AVE migration; *Cripto* mutations have AVE migration defects (D'Andrea et al., 2008). 4. *Otx2* expression is altered in *Pign* and *Pgap1* mutants; *Cripto* genetically interacts with *Otx2* to specify the AVE (Kimura et al., 2001), 5. A percentage of *gnz* mutant embryos display gastrulation defects; homozygous *Cripto* null mutants display gastrulation defects (Ding et al., 1998). 6. Cripto/Nodal signaling is reduced in *Pign* and *Pgap1* mutant cells and TGFβ responsive genes are downregulated in *Pign* and *Pgap1* mutant embryos. These pieces of evidence support the hypothesis that Cripto is a key GPI-AP whose dysfunction leads to an HPE-like phenotype.

GPI biosynthesis mutant phenotypes are variable

$Pign^{gnz}$ and $Pgap1^{bkr}$ mutant embryos share similar phenotypes, but are remarkably different in some aspects. First, *gnz* mutant embryos display forebrain truncations while *bkr* mutants show no phenotype in the 129S1 background. Second, Hex-GFP shows differential patterns of expression with *gnz* embryos expressing GFP at approximately normal levels in the normal number of cells, albeit those cells are not in their correct position, whereas *bkr* mutants have an expanded population of Hex-GFP cells and those cells overexpress Hex-GFP. Third, TGFβ responsive gene expression is reduced in $Pign^{gnz}$ and $Pgap1^{bkr}$ mutant embryos but the specific genes that are downregulated show little overlap.

In part these differences may be related to genetic background differences as the penetrance and severity of the developmental defects depends on the genetic background. These differences may also relate to the allele generated by the point mutations. The $Pgap1^{bkr}$ allele causes an in-frame deletion of 13 amino acids. $Pgap1^{bkr}$ mutant embryos in 129S1 background are morphologically normal, which suggests that $Pgap1^{bkr}$ retains partial activity. In contrast, $Pign^{gnz}$ is predicted to encode a truncated protein that both lacks catalytic activity and is not localized to the ER. $Pign^{gnz}$ phenotypes are influenced by genetic background but abnormal embryonic development is observed in all tested backgrounds.

The phenotypic differences may also relate to the different steps in GPI biosynthesis that Pign and Pgap1 catalyze. Pign catalyzes an early step in GPI biosynthesis, and disruption of *Pign* in cell lines leads to formation of several divergent GPI anchors, some of which localize to the plasma membrane, while others do not (Hong et al., 1999). Pgap1 catalyzes inositol deacylation after the GPI anchor is covalently bound to target proteins (Tanaka et al., 2004). Acyl-group removal is necessary for efficient ER export via CopII coated vesicles, and *Pgap1* mutant cells accumulate GPI-APs within the ER (Tanaka et al., 2004). As $Pign^{gnz}$ likely represents a null allele and Pign catalyzes a relatively early biosynthetic step in GPI anchor production, $Pign^{gnz}$ mutants likely represent a more severe class of GPI biosynthesis mutants than $Pgap1^{bkr}$ mutants. Alternatively, although the GPI biosynthesis pathway is largely thought to follow a linear progression, our *in vivo* results might suggest divergent requirements for this pathway in regulating various GPI-APs.

Cell autonomous vs. non-cell autonomous Cripto signaling

The contribution of cell autonomous versus non-cell autonomous Cripto/Nodal signaling is poorly understood. Lack of both cell autonomous and non-autonomous Cripto signaling results in a "head-without-trunk" phenotype (Ding et al., 1998). *Gnz* and *bkr* mutants, which present as a "trunk-without-head", likely retain some non-cell autonomous Cripto signaling while lacking cell autonomous Cripto signaling. Further, overexpression of a soluble form of Cripto can rescue zebrafish Oep mutants (Zhang et al., 1998). While cell autonomous Cripto signaling is clearly required for normal development, further studies are required to determine the role of non-cell autonomous Cripto signaling during early development.

Downstream effectors of forebrain development

Nodal/Cripto signaling is important for forebrain development, yet the downstream targets of this pathway are unknown. Analysis of genes that are altered in *gnz* and *bkr* mutants may shed light upon downstream effectors that mediate this process. *Col1a2* and *Il6* are significantly downregulated in *gnz* and *bkr* mutants; however, phenotypes associated with mutation of these genes in humans are unrelated to forebrain development (Dickson et al., 1984; Wirtz et al., 1987; Kishimoto, 2005). Three genes involved in iron homeostasis are either downstream of TGFβ signaling or GPI-APs. *Gdf2* and *Il6* converge to regulate expression of *Hepcidin* (Truksa et al., 2007), a key regulator of iron homeostasis (Nemeth and Ganz, 2009). The GPI-AP *Hemojuvelin* also regulates *Hepcidin*, so *gnz* and *bkr* mutants may have alterations in the function of genes that regulate iron levels. Iron levels are important for forebrain development in mice and mutation of the iron transporter Ferroportin causes anterior truncations (Mao et al., 2010). It will be interesting to test whether iron homeostasis is dysregulated in *bkr* and *gnz* mutants and, if so, this could provide a context to begin to understand the molecular relationships between different pathways that alter early forebrain development.

In humans, there is no current evidence linking mutations in GPI biosynthesis genes with HPE or forebrain truncations. Our studies raise the intriguing possibility that the ~thirty GPI biosynthesis enzymes may represent a new class of genes to test for linkage to holoprosencephaly, or other cranio-facial syndromes, such as agnathia, dysgnathia, microphthalmia and otocephaly.

Acknowledgements

We thank Kathryn Anderson, Elizabeth Lacy, Monica Justice and their labs for ENU mutagenesis; Trevor Williams, Weiguo Feng and Gartz Hanson for help with the forward genetic screen; Andy Peterson for sharing unpublished results; Kat Hadjantonakis (GPI-GFP), Tristan Rodriquez (Hex-GFP) and Michael Shen (Cripto plasmids) for mice and reagents, and David Clouthier for help interpreting skull morphologies. This project was supported by NINDS F31NS060454 and NICHD U01 HD043478. The content is solely the responsibility of the authors and does not necessarily represent the official views of the National Institute of Neurological Disorders And Stroke or the National Institutes of Health. L.N. is an investigator of the Howard Hughes Medical Institute.

Competing Interests

The authors have no competing interests to declare.

References

Allen, B. L., Tenzen, T. and McMahon, A. P. (2007). The Hedgehog-binding proteins Gas1 and Cdo cooperate to positively regulate Shh signaling during mouse development. *Genes Dev.* **21**, 1244-1257.

Andersson, O., Reissmann, E., Jörnvall, H. and Ibáñez, C. F. (2006). Synergistic interaction between Gdf1 and Nodal during anterior axis development. *Dev. Biol.* **293**, 370-381.

Chazaud, C. and Rossant, J. (2006). Disruption of early proximodistal patterning and AVE formation in Apc mutants. *Development* **133**, 3379-3387.

Chu, J. and Shen, M. M. (2010). Functional redundancy of EGF-CFC genes in epiblast and extraembryonic patterning during early mouse embryogenesis. *Dev. Biol.* **342**, 63-73.

Chu, J., Ding, J., Jeays-Ward, K., Price, S. M., Placzek, M. and Shen, M. M. (2005). Non-cell-autonomous role for Cripto in axial midline formation during vertebrate embryogenesis. *Development* **132**, 5539-5551.

Collignon, J., Varlet, I. and Robertson, E. J. (1996). Relationship between asymmetric nodal expression and the direction of embryonic turning. *Nature* **381**, 155-158.

D'Andrea, D., Liguori, G. L., Le Good, J. A., Lonardo, E., Andersson, O., Constam, D. B., Persico, M. G. and Minchiotti, G. (2008). Cripto promotes A-P axis specification independently of its stimulatory effect on Nodal autoinduction. *J. Cell Biol.* **180**, 597-605.

de la Cruz, J. M., Bamford, R. N., Burdine, R. D., Roessler, E., Barkovich, A. J., Donnai, D., Schier, A. F. and Muenke, M. (2002). A loss-of-function mutation in the CFC domain of TDGF1 is associated with human forebrain defects. *Hum. Genet.* **110**, 422-428.

Dickson, L. A., Pihlajaniemi, T., Deak, S., Pope, F. M., Nicholls, A., Prockop, D. J. and Myers, J. C. (1984). Nuclease S1 mapping of a homozygous mutation in the carboxyl-propeptide-coding region of the pro alpha 2(I) collagen gene in a patient with osteogenesis imperfecta. *Proc. Natl. Acad. Sci. USA* **81**, 4524-4528.

Ding, J., Yang, L., Yan, Y. T., Chen, A., Desai, N., Wynshaw-Boris, A. and Shen, M. M. (1998). Cripto is required for correct orientation of the anterior-posterior axis in the mouse embryo. *Nature* **395**, 702-707.

Gaynor, E. C., Mondésert, G., Grimme, S. J., Reed, S. I., Orlean, P. and Emr, S. D. (1999). MCD4 encodes a conserved endoplasmic reticulum membrane protein essential for glycosylphosphatidylinositol anchor synthesis in yeast. *Mol. Biol. Cell* **10**, 627-648.

Gritsman, K., Zhang, J., Cheng, S., Heckscher, E., Talbot, W. S. and Schier, A. F. (1999). The EGF-CFC protein one-eyed pinhead is essential for nodal signaling. *Cell* **97**, 121-132.

Hong, Y., Maeda, Y., Watanabe, R., Ohishi, K., Mishkind, M., Riezman, H. and Kinoshita, T. (1999). Pig-n, a mammalian homologue of yeast Mcd4p, is involved in transferring phosphoethanolamine to the first mannose of the glycosylphosphatidylinositol. *J. Biol. Chem.* **274**, 35099-35106.

Hoodless, P. A., Pye, M., Chazaud, C., Labbé, E., Attisano, L., Rossant, J. and Wrana, J. L. (2001). FoxH1 (Fast) functions to specify the anterior primitive streak in the mouse. *Genes Dev.* **15**, 1257-1271.

Juriloff, D. M., Sulik, K. K., Roderick, T. H. and Hogan, B. K. (1985). Genetic and developmental studies of a new mouse mutation that produces otocephaly. *J. Craniofac. Genet. Dev. Biol.* **5**, 121-145.

Kawagoe, K., Kitamura, D., Okabe, M., Taniuchi, I., Ikawa, M., Watanabe, T., Kinoshita, T. and Takeda, J. (1996). Glycosylphosphatidylinositol-anchor-deficient mice: implications for clonal dominance of mutant cells in paroxysmal nocturnal hemoglobinuria. *Blood* **87**, 3600-3606.

Kimura, C., Shen, M. M., Takeda, N., Aizawa, S. and Matsuo, I. (2001). Complementary functions of Otx2 and Cripto in initial patterning of mouse epiblast. *Dev. Biol.* **235**, 12-32.

Kimura-Yoshida, C., Nakano, H., Okamura, D., Nakao, K., Yonemura, S., Belo, J. A., Aizawa, S., Matsui, Y. and Matsuo, I. (2005). Canonical Wnt signaling and its antagonist regulate anterior-posterior axis polarization by guiding cell migration in mouse visceral endoderm. *Dev. Cell* **9**, 639-650.

Kinoshita, T., Fujita, M. and Maeda, Y. (2008). Biosynthesis, remodelling and functions of mammalian GPI-anchored proteins: recent progress. *J. Biochem.* **144**, 287-294.

Kishimoto, T. (2005). Interleukin-6: from basic science to medicine–40 years in immunology. *Annu. Rev. Immunol.* **23**, 1-21.

Lagutin, O. V., Zhu, C. C., Kobayashi, D., Topczewski, J., Shimamura, K., Puelles, L., Russell, H. R., McKinnon, P. J., Solnica-Krezel, L. and Oliver, G. (2003). Six3 repression of Wnt signaling in the anterior neuroectoderm is essential for vertebrate forebrain development. *Genes Dev.* **17**, 368-379.

Liguori, G. L., Borges, A. C., D'Andrea, D., Liguoro, A., Gonçalves, L., Salgueiro, A. M., Persico, M. G. and Belo, J. A. (2008). Cripto-independent Nodal signaling promotes positioning of the A-P axis in the early mouse embryo. *Dev. Biol.* **315**, 280-289.

Lowe, L. A., Yamada, S. and Kuehn, M. R. (2001). Genetic dissection of nodal function in patterning the mouse embryo. *Development* **128**, 1831-1843.

Mao, J., McKean, D. M., Warrier, S., Corbin, J. G., Niswander, L. and Zohn, I. E. (2010). The iron exporter ferroportin 1 is essential for development of the mouse embryo, forebrain patterning and neural tube closure. *Development* **137**, 3079-3088.

Maydan, G., Noyman, I., Har-Zahav, A., Neriah, Z. B., Pasmanik-Chor, M., Yeheskel, A., Albin-Kaplanski, A., Maya, I., Magal, N., Birk, E. et al. (2011). Multiple congenital anomalies-hypotonia-seizures syndrome is caused by a mutation in PIGN. *J. Med. Genet.* **48**, 383-389.

Mesnard, D., Guzman-Ayala, M. and Constam, D. B. (2006). Nodal specifies embryonic visceral endoderm and sustains pluripotent cells in the epiblast before overt axial patterning. *Development* **133**, 2497-2505.

Minchiotti, G., Parisi, S., Liguori, G., Signore, M., Lania, G., Adamson, E. D., Lago, C. T. and Persico, M. G. (2000). Membrane-anchorage of Cripto protein by glycosylphosphatidylinositol and its distribution during early mouse development. *Mech. Dev.* **90**, 133-142.

Ming, J. E. and Muenke, M. (2002). Multiple hits during early embryonic development: digenic diseases and holoprosencephaly. *Am. J. Hum. Genet.* **71**, 1017-1032.

Muenke, M. and Beachy, P. A. (2000). Genetics of ventral forebrain development and holoprosencephaly. *Curr. Opin. Genet. Dev.* **10**, 262-269.

Mukhopadhyay, M., Shtrom, S., Rodriguez-Esteban, C., Chen, L., Tsukui, T., Gomer, L., Dorward, D. W., Glinka, A., Grinberg, A., Huang, S. P. et al. (2001). Dickkopf1 is required for embryonic head induction and limb morphogenesis in the mouse. *Dev. Cell* **1**, 423-434.

Nemeth, E. and Ganz, T. (2009). The role of hepcidin in iron metabolism. *Acta Haematol.* **122**, 78-86.

Nomura, M. and Li, E. (1998). Smad2 role in mesoderm formation, left-right patterning and craniofacial development. *Nature* **393**, 786-790.

Paulick, M. G. and Bertozzi, C. R. (2008). The glycosylphosphatidylinositol anchor: a complex membrane-anchoring structure for proteins. *Biochemistry* **47**, 6991-7000.

Perea-Gomez, A., Vella, F. D., Shawlot, W., Oulad-Abdelghani, M., Chazaud, C., Meno, C., Pfister, V., Chen, L., Robertson, E., Hamada, H. et al. (2002). Nodal antagonists in the anterior visceral endoderm prevent the formation of multiple primitive streaks. *Dev. Cell* **3**, 745-756.

Rhee, J. M., Pirity, M. K., Lackan, C. S., Long, J. Z., Kondoh, G., Takeda, J. and Hadjantonakis, A. K. (2006). *In vivo* imaging and differential localization of lipid-modified GFP-variant fusions in embryonic stem cells and mice. *Genesis* **44**, 202-218.

Rodriguez, T. A., Casey, E. S., Harland, R. M., Smith, J. C. and Beddington, R. S. (2001). Distinct enhancer elements control Hex expression during gastrulation and early organogenesis. *Dev. Biol.* **234**, 304-316.

Rodriguez, T. A., Srinivas, S., Clements, M. P., Smith, J. C. and Beddington, R. S. (2005). Induction and migration of the anterior visceral endoderm is regulated by the extra-embryonic ectoderm. *Development* **132**, 2513-2520.

Rohr, K. B., Barth, K. A., Varga, Z. M. and Wilson, S. W. (2001). The nodal pathway acts upstream of hedgehog signaling to specify ventral telencephalic identity. *Neuron* **29**, 341-351.

Song, J., Oh, S. P., Schrewe, H., Nomura, M., Lei, H., Okano, M., Gridley, T. and Li, E. (1999). The type II activin receptors are essential for egg cylinder growth, gastrulation, and rostral head development in mice. *Dev. Biol.* **213**, 157-169.

Stuckey, D. W., Clements, M., Di-Gregorio, A., Senner, C. E., Le Tissier, P., Srinivas, S. and Rodriguez, T. A. (2011). Coordination of cell proliferation and anterior-posterior axis establishment in the mouse embryo. *Development* **138**, 1521-1530.

Takaoka, K., Yamamoto, M. and Hamada, H. (2011). Origin and role of distal visceral endoderm, a group of cells that determines anterior-posterior polarity of the mouse embryo. *Nat. Cell Biol.* **13**, 743-752.

Tanaka, S., Maeda, Y., Tashima, Y. and Kinoshita, T. (2004). Inositol deacylation of glycosylphosphatidylinositol-anchored proteins is mediated by mammalian PGAP1 and yeast Bst1p. *J. Biol. Chem.* **279**, 14256-14263.

Topczewski, J., Sepich, D. S., Myers, D. C., Walker, C., Amores, A., Lele, Z., Hammerschmidt, M., Postlethwait, J. and Solnica-Krezel, L. (2001). The zebrafish glypican knypek controls cell polarity during gastrulation movements of convergent extension. *Dev. Cell* **1**, 251-264.

Tremml, G., Dominguez, C., Rosti, V., Zhang, Z., Pandolfi, P. P., Keller, P. and Bessler, M. (1999). Increased sensitivity to complement and a decreased red blood cell life span in mice mosaic for a nonfunctional Piga gene. *Blood* **94**, 2945-2954.

Truksa, J., Peng, H., Lee, P. and Beutler, E. (2007). Different regulatory elements are required for response of hepcidin to interleukin-6 and bone morphogenetic proteins 4 and 9. *Br. J. Haematol.* **139**, 138-147.

Ueda, Y., Yamaguchi, R., Ikawa, M., Okabe, M., Morii, E., Maeda, Y. and Kinoshita, T. (2007). PGAP1 knock-out mice show otocephaly and male infertility. *J. Biol. Chem.* **282**, 30373-30380.

Varlet, I., Collignon, J. and Robertson, E. J. (1997). nodal expression in the primitive endoderm is required for specification of the anterior axis during mouse gastrulation. *Development* **124**, 1033-1044.

Vincent, M. J., Martin, A. S. and Compans, R. W. (1998). Function of the KKXX motif in endoplasmic reticulum retrieval of a transmembrane protein depends on the length and structure of the cytoplasmic domain. *J. Biol. Chem.* **273**, 950-956.

Watanabe, K., Hamada, S., Bianco, C., Mancino, M., Nagaoka, T., Gonzales, M., Bailly, V., Strizzi, L. and Salomon, D. S. (2007). Requirement of glycosylphosphatidylinositol anchor of Cripto-1 for trans activity as a Nodal co-receptor. *J. Biol. Chem.* **282**, 35772-35786.

Wirtz, M. K., Glanville, R. W., Steinmann, B., Rao, V. H. and Hollister, D. W. (1987). Ehlers-Danlos syndrome type VIIB. Deletion of 18 amino acids comprising the N-telopeptide region of a pro-alpha 2(I) chain. *J. Biol. Chem.* **262**, 16376-16385.

Yamamoto, M., Meno, C., Sakai, Y., Shiratori, H., Mochida, K., Ikawa, Y., Saijoh, Y. and Hamada, H. (2001). The transcription factor FoxH1 (FAST) mediates Nodal signaling during anterior-posterior patterning and node formation in the mouse. *Genes Dev.* **15**, 1242-1256.

Yamamoto, M., Saijoh, Y., Perea-Gomez, A., Shawlot, W., Behringer, R. R., Ang, S. L., Hamada, H. and Meno, C. (2004). Nodal antagonists regulate formation of the anteroposterior axis of the mouse embryo. *Nature* **428**, 387-392.

Yan, Y.-T., Liu, J.-J., Luo, Y., E, C., Haltiwanger, R. S., Abate-Shen, C. and Shen, M. M. (2002). Dual roles of Cripto as a ligand and coreceptor in the nodal signaling pathway. *Mol. Cell. Biol.* **22**, 4439-4449.

Ye, S., Dhillon, S., Ke, X., Collins, A. R. and Day, I. N. (2001). An efficient procedure for genotyping single nucleotide polymorphisms. *Nucleic Acids Res.* **29**, e88.

Zhang, J., Talbot, W. S. and Schier, A. F. (1998). Positional cloning identifies zebrafish one-eyed pinhead as a permissive EGF-related ligand required during gastrulation. *Cell* **92**, 241-251.

Zoltewicz, J. S., Plummer, N. W., Lin, M. I. and Peterson, A. S. (1999). oto is a homeotic locus with a role in anteroposterior development that is partially redundant with Lim1. *Development* **126**, 5085-5095.

Zoltewicz, J. S., Ashique, A. M., Choe, Y., Lee, G., Taylor, S., Phamluong, K., Solloway, M. and Peterson, A. S. (2009). Wnt signaling is regulated by endoplasmic reticulum retention. *PLoS ONE* **4**, e6191.